Erkan and Balkan-Pazvantoğlu
Geothermal Energy (2023) 11:13
https://doi.org/10.1186/s40517-023-00253-7

Geothermal Energy

RESEARCH Open Access

Distribution of surface heat flow and effects on the subsurface temperatures in the northern part of Thrace Basin, NW Turkey

Kamil Erkan[1*] and Elif Balkan-Pazvantoğlu[2]

*Correspondence:
kamil.erkan@marmara.edu.tr

[1] Department of Environmental Engineering, Marmara University, Maltepe, Istanbul, Turkey
[2] Department of Geophysical Engineering, Dokuz Eylül University, Buca, Izmir, Turkey

Abstract

The Thrace Basin in northwestern Turkey is a deep Eocene–Oligocene hydrocarbon-bearing sedimentary basin. The basin has potential for geothermal energy utilization in the future due to its favorable geological conditions. In this study, we combined the available bottom hole temperature (BHT) data from 70 points with the thermal conductivity and radiogenic heat productions of the basin formations, and generated a detailed thermal model of the northern part of the basin. For heat flow determinations from the BHT data, we applied Bullard's thermal resistance method on formation thermal conductivities and thicknesses. The results give an average surface heat flow of 65.8 ± 11.3 mW/m^2. We obtained high heat flow values (75–80 mW/m^2) in the eastern and western sides, and the central part of the study area. These relatively high heat flow values can be explained by the combined effect of basement topography and the variations in the radiogenic heat production of the basement rocks. The calculated subsurface temperatures in selected hydrocarbon fields vary in the range of 45–64 °C at 1 km depth, 99–136 °C at 3 km depth, and 155–208 °C at 5 km depth as a result of local variations of the surface heat flow and formation thermal resistances. These variations in subsurface temperatures can have significant effects on the cost of geothermal energy production in future.

Keywords: Heat flow, Thrace Basin, Geothermal, Bottom-hole temperature, Bullard's method

Introduction

Understanding thermal regimes of sedimentary basins are significant in many ways including hydrocarbon maturation processes (Yalçın 1991) and the geothermal energy potential of sedimentary formations (Tester et al. 2006). Geothermal energy from sedimentary formations (hot aquifers) has already been exploited for direct uses (e.g., Lopez et al. 2010), and for power production (e.g., Eyerer et al. 2020). With the increasing demand for renewable energy sources, many sedimentary basins worldwide have potential for development (Allis et al. 2015; Limberger et al. 2018). Furthermore, in hydrologically unfavorable areas, artificial reservoirs can be made for efficient geothermal energy production by today's new drilling and fracturing methods (collectively called enhanced

geothermal systems—EGS). It has been argued that the existing infrastructure in sedimentary basins due to oil–gas explorations can significantly decrease the cost of geothermal energy production in sedimentary basins (Tester et al. 2006).

Assuming a constant basal heat flow from the mantle, important factors that control the thermal state of a sedimentary basin are the thermal conductivities of sedimentary formations (i.e., shale contents), and radiogenic heat production of the basement rocks (Blackwell and Steele 1989). These factors collectively are measured as the surface heat flow, which is the primary parameter for calculating subsurface temperatures. The Thrace Basin is interesting due to the existence of thick shale-dominated formations such as Ceylan formation and possible heat-producing (i.e., granitic) rocks at the basement, as they are extensively manifested in the Strandja massif in the north of the basin (Şahin et al. 2014). In the heat flow map of Turkey (Tezcan and Turgay 1991; also see Tezcan 1999), the Thrace basin is broadly represented by high heat flow values (70–80 mW/m^2). In a previous thermal study, Huvaz et al. (2007) calculated the geothermal gradient distribution in the basin using bottom-hole temperatures (BHT) from hydrocarbon wells by assuming uniform thermal properties for the formations. They also emphasized the effect of basin thermal refraction on the distribution of geothermal gradients. Similarly, Başel et al. (2010) calculated temperature distribution at 1000 m depth by spatial interpolation of the BHT data. However, previous studies did not take the variations in the thermal properties of the basin formations (i.e., thermal conductivity and radiogenic heat generation values) into account on a regional basis. The aim of this study is to generate a detailed thermal model of the northern Thrace Basin using the available BHT data along with the available thermal conductivity, radiogenic heat production, and sedimentary thickness data obtained during hydrocarbon explorations.

For modeling the regional thermal regime, surface heat flow is a more powerful parameter than the geothermal gradient, as the latter can be disturbed by the local variations in thermal conductivity values of rocks (Blackwell and Steele 1989; Beardsmore and Cull 2001). Furthermore, the surface heat flow can be directly used to calculate formation temperatures at depth for any point in the basin using formation thermal conductivity, radiogenic heat production values, and formation thickness information. Using this approach, we calculated formation temperatures for deep wells in the several hydrocarbon fields in the basin.

Geological setting

Thrace Basin in the northwestern Turkey is an Eocene–Oligocene sedimentary basin having significant hydrocarbon deposits (Siyako and Huvaz 2007; Perinçek et al. 2015). It is bounded by the Strandja Massif in the north; its southern boundary is not well defined but it goes beyond the Sea of Marmara (Fig. 1). Extensive drilling activities as part of hydrocarbon explorations show that the basin is underlain by the metamorphic/granitic rocks of the Strandja massif to the North Anatolian Fault in the south (Okay et al. 2010). These metamorphic/granitic rocks are formed during Permian to Jurassic by continental collision in the region (Okay et al. 2001). Görür and Okay (1996) suggested that the basin developed as a fore-arc basin during the northward subduction of the western branch of the Intra-Pontide ocean during the Eocene

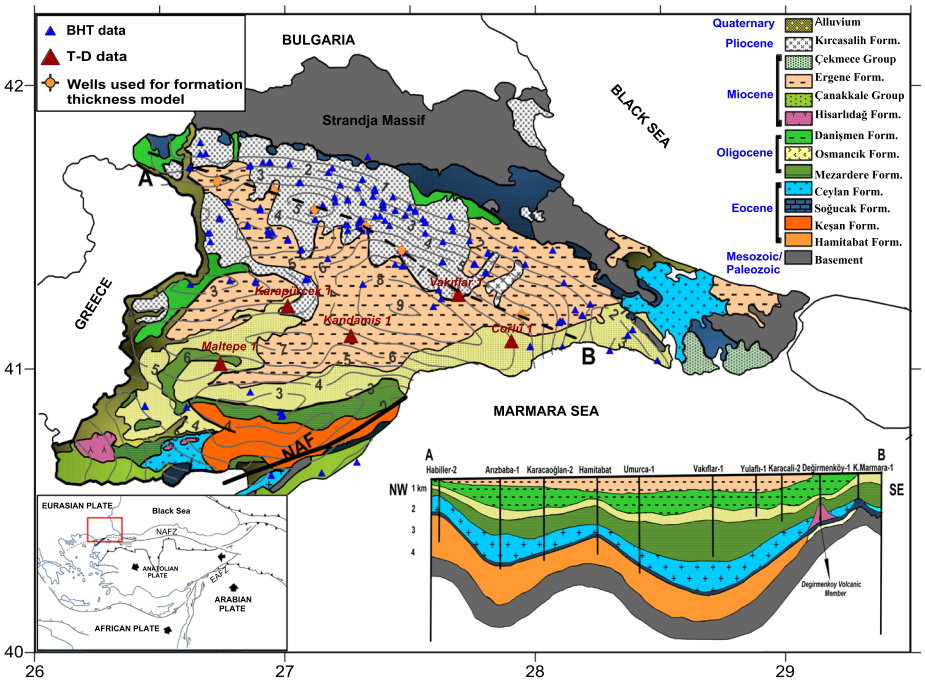

Fig. 1 Geological map of the Thrace basin (Siyako and Huvaz 2007) and the distribution of the available temperature/depth data. Basin depths are also shown as contour lines for each kilometer (also from Siyako and Huvaz 2007). The geological cross section (**A**–**B**) was taken from Gürgey (2009)

and Oligocene. The Thrace region was under the influence of Aegean subduction zone by volcanic activity during the Oligocene–Early Miocene; this was the last tectonothermal event, as manifested by the mafic to intermediate volcanic rocks observed within the basin formations (Yılmaz and Polat 1998). The petrology of the volcanic rocks also suggests that the basin experienced extensional tectonics as the back arc of the Aegean subduction zone during this period. Trans-tensional faults (now inactive) within the basin were interpreted as the northern branch of the North Anatolian Fault zone that was active during the Miocene (Perinçek 1991).

Thrace Basin formations can be grouped into three age groups that are Miocene/Pliocene, Oligocene, and Eocene ages (Siyako and Huvaz 2007; Perinçek et al. 2015). The ages and spatial distribution of these formations are shown in Fig. 1 along with a thickness profile in the inset of Fig. 1. Miocene/Pliocene groups are mostly fluvial in origin. Ergene formation mostly consists of sandstones and conglomerates and has good aquifer conditions (Ökten and Yazıcıgil 2005). Oligocene Danişmen, Osmancık and Mezardere formations consist of sandstones, shales, and siltstones and show delta/delta front environmental conditions. Osmancık and Danişmen formations also bear significant coal deposits (Perinçek et al. 2015). The Eocene age formations include Ceylan, Soğucak, and Hamitabat formations have dominantly shale, limestone and sandstone-dominated lithologies, respectively, and show proximal and distal turbidite environmental conditions. In the Thrace Basin, Eocene Hamitabat and Oligocene Mezardere formations are considered to be the source rocks of the hydrocarbon deposits.

Available thermal data

The primary data set used in this study come from BHT measurements, which are especially widespread in the northern Thrace Basin (see Fig. 1). In this study, we only used data from references, where individual temperature/depth pairs with location information were reported (total of 70 points, mostly from Uzunlar 2006; and some data from Huvaz 2005 and Huvaz et al. 2005). Since the BHT data is mostly located in the northern parts, we limited our analysis in the northern part of the basin. The BHT data were obtained during or just after drilling as individual temperature-vs-depth pairs. Depending on the type of acquisition method the data may include a correction for thermal disturbance based on formulas for the thermal effect of drilling fluid circulation (Beardsmore and Cull 2001; Mıhçakan et al. 2006). As a result of this, errors for BHT data are usually not bounded and an independent check with equilibrium temperature–depth (T–D) in the same area is needed (see below). In the Thrace Basin, equilibrium T–D logs from deep wells were reported at five locations by Pfister et al. (1998); their locations are shown in Fig. 1 as ruby color triangles. In addition, Pfister et al. (1998) also reported heat flow values from equilibrium T–D data from several shallow wells within the shallow aquifer (Ökten and Yazıcıgil 2005). Since these data include assumptions for corrections of the hydrological activity, they were not included in this study.

A comparison of the available BHT and equilibrium T–D data from deep wells is shown in Fig. 2a. A general agreement between the two data sets shows that the BHT data can be used for further thermal modeling analysis. A least-squares fit (red line) to the BHT gives an average geothermal gradient of 34.3 °C/km for the Northern Thrace basin.

Figure 2b shows the same equilibrium T–D curves with more details. By comparison of the T–D data, we interpret that two wells (Maltepe-1 and Kanmadis-1) show

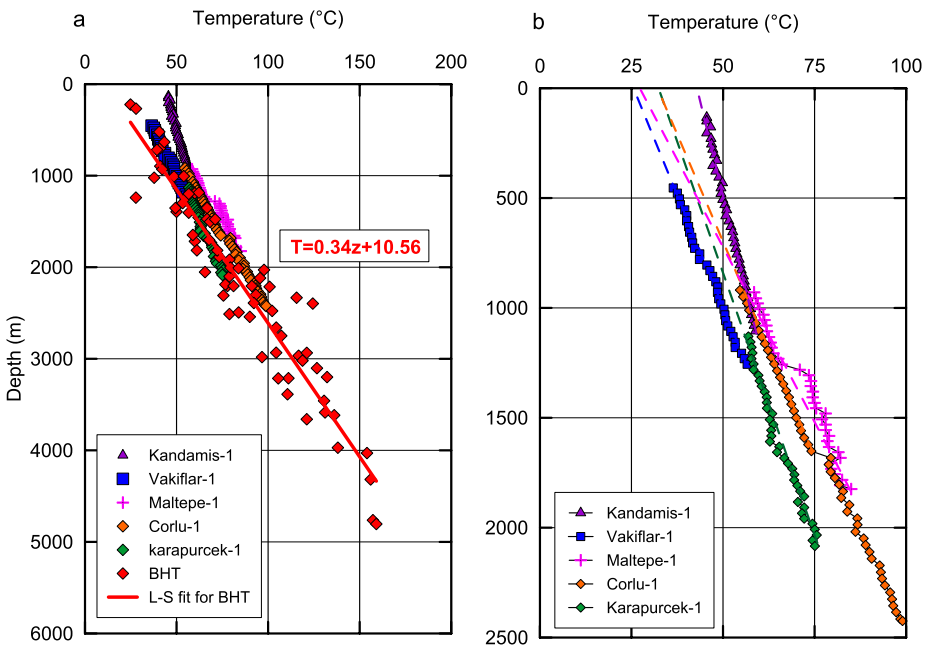

Fig. 2 **a** Comparison of BHT and equilibrium T–D data; **b** Equilibrium T–D logs shown with extrapolations to the ground surface

intra-borehole fluid flow activity in some sections, where measured temperatures are higher than formation temperatures as a result of rising of warmer fluids from deeper levels to shallower levels (Jessop 1990; Erkan 2015). In Maltepe-1, an upflow from the bottom of the well to depth of ~ 1300 m results in temperatures higher than the formation temperatures within the interval. For Kandamis-1, the fact that the extrapolated surface temperature is unrealistically high (~ 44 °C) indicates that the intra-borehole upflow is effective for the entire of the measured interval. Both of these wells are outside of the study area, and were not used in further analyses. These intra-borehole fluid flow activities are only effective within the borehole in certain intervals and heat flow outside of these intervals is still conductive. For the remaining wells, geothermal gradients are calculated as 28.05 °C/km for Çorlu-1 (between 1773 and 2425 m), 24.26 °C/km for Vakiflar-1, and 20.43 °C/km for Karapurcek-1. In Corlu-1, the cause of the break at 1745 m depth is interpreted to be due to an instrumental calibration problem.

As seen by the dashed lines in Fig. 2b, all of the equilibrium T–D curves extrapolate to surface temperature values that are higher than the mean annual surface temperature of the region (~ 15 °C; Şensoy et al. 2008). According to the theory of one-dimensional heat conduction, this implies low thermal conductivities for formations at shallow depths. Interestingly, this behavior is observed even outside of the shallow aquifer, where low-permeability Oligocence/Econe units (0.1–10 m-Darcy; Siyako and Huvaz 2007; also see Ökten and Yazıcıgil 2005) are exposed at the surface (see, for example, Maltepe-1 and Karapurcek-1 in Figs. 1 and 2). The inferred low thermal conductivities at shallow depths may be either a result of high porosities of shallow units (e.g., Ergene formation, Ökten and Yazıcıgil 2005) or effect of massive lignite layers (with thermal conductivities as low as 0.18 W/m/K; Clark 1966) available in Osmancık and Danişmen formations (Perinçek et al. 2015). The existence of such a thermal conductivity layer at shallow depths (0–500 m) can have significant effects on deep temperatures as a results of high geothermal gradients, and part of the differences in temperatures at depth can be explained by variations of the thickness of this layer within the basin. However, in this study, we constrain deep (> 1 km) formation temperatures by the deep BHT data, so the details of the shallow thermal conditions are not needed for the analyses.

Average thermal conductivities of the sedimentary formations used in this study were previously reported by Huvaz et al. (2005) on 321 core samples from 46 wells (Table 1). According to this, thermal conductivities vary between 1.76 and 3.02 W/m/K; the lowest values belong to the shale dominated Ceylan formation, while the highest values belong to the sandstone/siltstone dominated Danişmen formation. These results are in agreement with the literature values of these lithologies (Beardsmore and Cull 2001; Balkan et al. 2017). The average radiogenic heat productions of formations were obtained from gamma-ray logs reported in various papers given in the footnote of Table 1.

For three formations in Table 1, thermal conductivity measurements are not available (Ergene, Osmancık, and Soğucak formations). Values for these formations were assigned by their lithological descriptions given in Huvaz et al. (2005) (see Table 1). According to this, Soğucak formation is composed of shallow marine limestone (Siyako and Huvaz 2007), and a generic value of 3.4 W/m/K for neritic limestone was used (Balkan et al. 2017). Danişmen and Osmancık formations have similar lithological properties to each other (Perinçek et al. 2015), so a similar thermal conductivity was used for Osmancık

Table 1 Thermal and lithological properties of the formations in Thrace Basin

Formation name	λ[a] (N/W)	A[b]	Lithologic description[c]	Ave. percent thickness[d]
Ergene	1.5 (est)	0.7	Sandstone + conglomerate	–
Danişmen	3.02 (65/2)	0.8	Shale + siltstone	18 ± 6
Osmancık	3.1 (est)	0.8	Shale + sandstone	9 ± 2
Mezardere	2.86 (54/3)	0.8	Shale + sandstone	20 ± 6
Ceylan	1.76 (73/8)	0.8	Shale	21 ± 8
Ceylan (tuff)	0.95 (38/2)	1.1	Tuff	~0
Soğucak	3.4 (est)	0.3	Limestone + shale	3 ± 1
Hamitabat (shallow)	2.42 (55/13)	1.1	Sandstone + shale	29 ± 10
Hamitabat (deep)	2.89 (29/18)	1.1	Sandstone + shale	

[a] λ: thermal conductivity (W/m/K); N: number of samples; W: number of wells (Huvaz et al. 2005). "est" means estimated, see the text for details

[b] A: heat generation (μW/m^3); values based on gamma-ray logs (Coşkun 1997; Coşkun 2000; Siyako and Huvaz 2007; Turgut and Eseller 2000). Values were converted from API to SI units as in Beardsmore and Cull (2001)

[c] Huvaz et al. (2005)

[d] Average percent thickness of each formation calculated using well data in Gürgey (2009); see Fig. 1 inset, which is used in Bullard method. See the text for details

formation. Ergene formation which covers the top part of the most of the northern basin is dominantly sandstone and conglomerate and makes up the volume of the shallow aquifer in the basin (Ökten and Yazıcıgil 2005). Considering the high porosity of this unit, a low thermal conductivity value (1.5 W/m/K) for this formation was assigned. This value is constrained by the extrapolated annual surface temperature of the equilibrium T–D data in Fig. 2b.

Methods

Determination of heat flow requires the measurements of both geothermal gradient and thermal conductivity along a vertical rock column. Since our data set consists of BHT data, where temperature/depth values are given as single points, the effect of thermal conductivity of the overlying rock column on the temperature at depth can be best incorporated using the Bullard's thermal resistance method (Bullard 1939). Considering a BHT data point (z, T), the integrated thermal resistance (R) of the overlying rock column to the depth (z) is defined as

$$R = \sum_i \frac{h_i}{\lambda_i} \text{ and } z = \sum_i h_i \tag{1}$$

where λ_i and h_i are thermal conductivity and thickness of the ith formation over the depth of the BHT measurement, respectively. In the case of multiple T/D points, the graph of temperature-versus-thermal resistance is called a "Bullard plot". In the case of a single BHT point, heat flow (Q_0) is calculated as

$$Q_0 = \frac{(T - T_0)}{R} \tag{2}$$

where T_0 is the surface temperature at the location of the borehole. In Eq. 2, the Bullard plot is assumed to be linear which means the non-linearity due to radiogenic heat production is ignored. The non-linear term on subsurface temperatures due to radiogenic heat production is given as $Az^2/(2\lambda)$ (see Eq. 4). As an example, for an average heat production of 0.8 $\mu W/m^3$and $\lambda = 2$ W/m/K, at a depth of = 3 km, the effect of non-linearity on the temperature is calculated to be 1.8 °C. By Eqs. (1) and (2), we calculated the effect of non-linearity on the surface heat flow as 1.2 mW/m^2, which can conveniently be neglected.

For the calculation of the thermal resistance value (R) in Eq. 1, one also needs the thickness of each formation over the overlying column to the depth of measurement. Since this information for each individual BHT site is not available in the published resources, thicknesses were calculated based on a model. By comparing the formation thicknesses with the basement depths in the geological profile shown in Fig. 1 (see the inset) one observes that the they are proportional as a first-order approximation (also see, Doust and Arıkan 1974; Plate 6). Using the data from seven wells reported by Gürgey (2009; see Fig. 1 for well locations), we calculated the percent thickness of each formation with respect to the total thickness of the basin, as shown in Table 1. In percent thickness calculations, Ergene formation was excluded because of its continental (fluvial) origin and its recent erosion (Siyako and Huvaz 2007).

Formation thermal conductivity values in Table 1 represent surface conditions (T_0) and in-situ values would decrease with depth by increasing temperatures. To account for the temperature dependence of thermal conductivities at depth, the formula of Eppelbaum et al. (2014, Eq. 2.1.3) which is given exclusively for sedimentary formations up to 300 °C was used:

$$\lambda_T = \lambda_0 - (\lambda_0 - 3.3)\left[\exp\left(0.725\frac{T - T_0}{T + 130}\right) - 1\right] \tag{3}$$

here, λ_0 is the thermal conductivity of the sedimentary rock at (T_0), and λ_T is the thermal conductivity at temperature T. In resistance calculations in Eq. 2, temperature-dependent thermal conductivity of each formation was calculated using Eq. 3, where mean formation temperatures were calculated using the linear regression formula in Fig. 2a.

Results and discussion

The resulting Bullard plots for all BHT points based on the method given above are shown in Fig. 3. We calculated the surface heat flow by calculating the slope for each BHT point in Fig. 3 with respect to the ground surface temperature (15 °C). The resulting heat flow values are shown on the map in Fig. 4 by numbers next for each BHT point. We observe that all heat flow values fall in the range of 40–90 mW/m^2. Among these values 17 data points fall below 60 mW/m^2, 32 points fall in 60–70 mW/m^2, and 23 points fall higher than 70 mW/m^2. The average heat flow is calculated to be 65.8 ± 11.3 mW/m^2. A table of calculated heat flow values can be found in the supplementary document.

For spatial interpolation of the heat flow points and mapping, we gridded the data using the Kriging method with a grid interval of 0.15° by 0.15°; then, we applied 11-point Gaussian window smoothing to eliminate the local scatter in the heat flow variations. The purpose of using a large smoothing window was to eliminate the

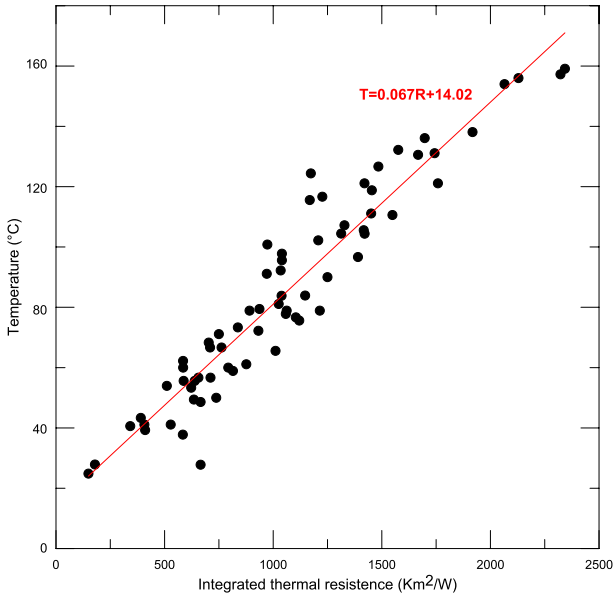

Fig. 3 Plot of the BHT data as a function of integrated thermal resistance of the overlying rock column (Bullard plot). The best-fit line in red color gives an average surface heat flow of 67 mW/m^2 and extrapolated ground surface temperature 14.2 °C

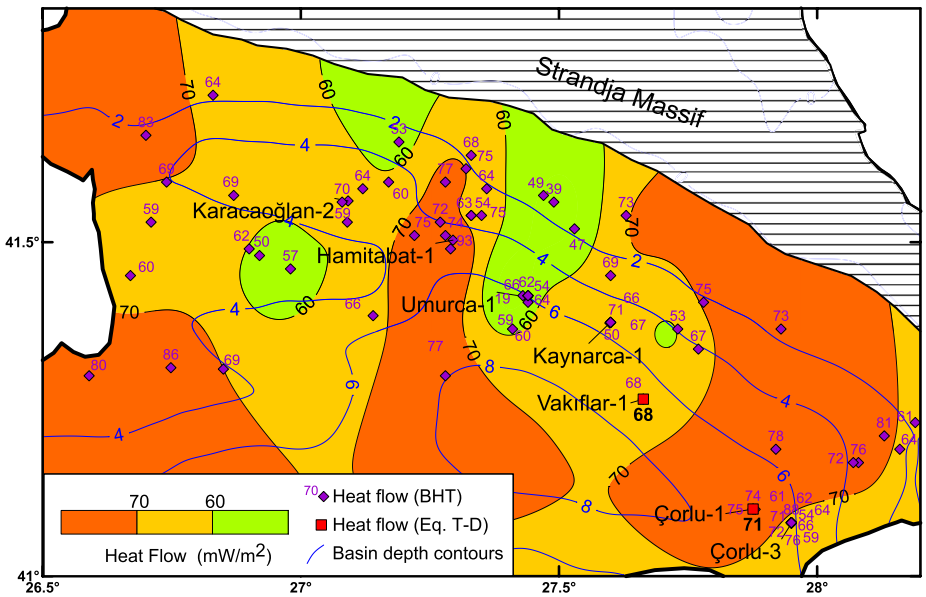

Fig. 4 Calculated heat flow values and a contour map showing the general variations of the surface heat flow in the Northern Thrace Basin. The mean of the residuals between calculated and interpolated heat flow values is 4.7 mW/m^2. Heat flow determinations from two equilibrium T–D data are given in bold

inherent scatter in the BHT data and decrease error in the heat flow results, which is routinely done in the processing of potential fields. For mapping the heat flow distribution, we divided the heat flow values into three intervals that are less than 60 mW/

m^2, between 60 and 70 mW/m^2, and higher than 70 mW/m^2. The resulting contour map of heat flow distribution is shown in Fig. 4.

The heat flow map in Fig. 4 shows that there are certain areas, where the surface heat flow is larger than 70 mW/m^2. These areas located in the eastern and western sides of the basin; and in the central part of the basin around the Hamitabat field. Assuming a constant mantle heat flow in the study area, these relatively high heat flow values can be explained by the combined effect of basement topography (see the 3D thermal model results below) and the variations in the radiogenic heat production of the basement rocks.

Synthetic T–D curves in selected fields

The availability of heat flow and thermal conductivity with a model for formation thicknesses allow us to generate synthetic T–D curves at any location in the basin. We selected several hydrocarbon exploration fields in the basin for this purpose (see Fig. 4 for their locations). The method of solution of the 1-D steady-state heat conduction equation is given by Chapman (1986; also Förster et al. 2021). In this method, the surface heat flow and the mean annual temperature are taken for a specific site, the subsurface is divided into finite thickness layers, and temperatures downward at the bottom of each layer are calculated, assuming that thermal conductivity and heat generation are constant within each layer. We used a layer thickness of 100 m in our calculations and continued our calculation down to 5000 m. The resulting T–D curves are shown in Fig. 5. In Fig. 5, the panel on the left (panel a) shows the results for sites with BHT data within the distance of 10 km from each site, and the panel on the right (panel b) shows sites, where equilibrium T–D data are available.

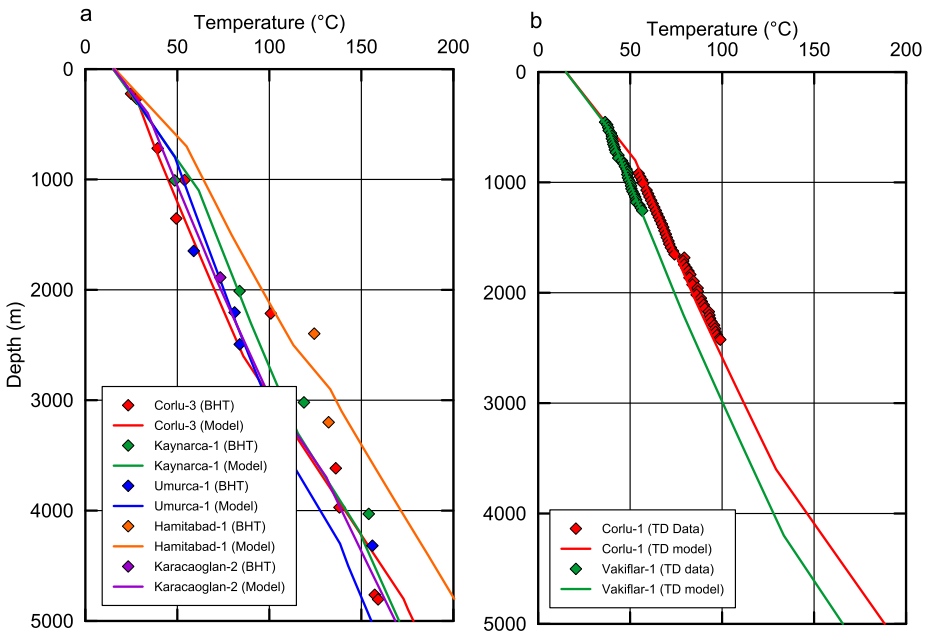

Fig. 5 Synthetic T–D curves for selected fields, where **a** BHT data only and **b** equilibrium T-D data are available. See Fig. 4 for locations of the fields

Calculated temperatures at certain depths extracted from the synthetic T–D curves are shown in Table 2. Formation temperatures vary in the ranges of 45–64 °C at 1 km, 99–136 °C at 3 km, and 155–208 °C at 5 km. Başel et al. (2010) reports temperatures of 45–55 °C at 1000 m-depth for the study area, which are within the range of our results at the same depth. Table 2 indicates even higher temperatures at some locations. Calculated temperature values in Table 2 reflect variations of both surface heat flow and thermal conductivity properties of the basin rocks. For example, Hamitabat-1 field shows high temperatures at 1 km depth as a result of high surface heat flow. We calculated the temperature of 208 ± 30 °C at 5 km here. On the other hand, Kaynarca-1 field shows also high temperatures at 1 km depth but this is a result of the thick low thermal conductivity layer there and not the surface heat flow. In this field, unlike Hamitabat-1, temperatures get lower values at greater depths in comparison with most of the other fields (see Fig. 5).

In Table 2, we also estimated the basement heat production values by assuming a constant mantle heat flow of 45 mW/m^2 (see the 3D thermal model below). The values are in the range of 1–3.2 $\mu W/m^3$. These values are in agreement with the measured values of 1.3–4.3 $\mu W/m^3$ in Strandja Massif by Aysal et al. (2018) and Şahin et al. (2014).

Effects of the basement structure

To investigate the impact of basin geometry on the surface heat flow we produced a 3-D thermal model of the northern Thrace Basin based on the solution of the steady-state heat conduction. Finite elements method-based numerical modeling software Comsol Multiphysics (TM) was used to obtain forward modeling results.

The final model contains four layers (Fig. 5) and covers a 240 km and 150 km area and extends vertically down to a depth of 30 km which is the mean crustal thickness estimated from geophysical studies (Ates et al. 2012; Karabulut et al. 2013). The basin depths, given in Fig. 1 are used to generate the sedimentary fill part of the model geometry. Based on the discussion above, a low thermal conductivity layer is also included for the first 500 m of the model. Thermal conductivities and heat production values for

Table 2 Calculated temperatures at certain depths for the selected fields

Field	Q_0 (mW/m^2)	h (m)	T@1 km (°C)	T@2 km (°C)	T@3 km (°C)	T@4 km (°C)	T@5 km (°C)	est-A ($\mu W/m^3$)
Corlu-1	71.0	700	58 ± 4	84 ± 7	112 ± 10	146 ± 13	188 ± 17	2.3
Corlu-3	67.4	200	45 ± 5	70 ± 12	102 ± 19	141 ± 24	178 ± 30	1.8
Hamitabat-1	83.8	600	64 ± 7	96 ± 12	136 ± 18	171 ± 24	208 ± 30	3.2
Karacaoglan-2	69.7	300	49 ± 5	74 ± 10	102 ± 15	139 ± 21	169 ± 26	2
Kaynarca-1	63.9	1000	57 ± 7	83 ± 12	108 ± 16	142 ± 22	171 ± 27	1
Umurca-1	61.3	700	53 ± 6	75 ± 10	99 ± 14	128 ± 20	155 ± 25	1.1
Vakıflar-1	68.0	400	50 ± 3	74 ± 6	100 ± 8	128 ± 11	166 ± 15	2

"h" refers to the thickness of the low-thermal conductivity layer that gives the best-fit with the data. Estimated basement heat productions (est-A) are calculated for a constant mantle heat flow of 45 mW/m^2 for all sites

related lithologies are populated from this study if they are available or complied from the previously published studies.

The thermal properties used in the model are given in Table 3. Thermal conductivity and heat production of the basin fill is calculated by weighting values given in Table 1 with thicknesses of formations. Temperature dependence of thermal conductivity in the basin fill is evaluated using Eq. 3 above. For the basement, the equation developed by Kukkonen et al. (1999) is used for the temperature dependence on thermal conductivity and the minor effect of pressure is ignored in our model.

Dirichlet boundary condition is fixed at 15 °C on the surface of the model, which is the annual mean temperature for the region (Şensoy et al. 2008). A constant mantle heat flow is set for the bottom of the model, while it is assumed that the sides of the model are thermally insulated implying no lateral heat flow. The aim of the model is to evaluate the best match between measured and modeled temperatures by providing a quantitative estimate of the mantle heat flow in the Thrace basin. For the thermal model validation, the calculated temperatures are compared to temperatures measured in the wells, which show good agreement with each other using a mantle heat flow of 45 mW/m^2 in Fig. 6. The standard error for the misfit is calculated to be 10 °C.

Figure 7a shows the effect of thermal refraction of the mantle heat flow only due to the basin topography. Heat flow variation between the basin and Strandja massif is about 3 mW/m^2. When the heat production rate of the basement rocks is included in our calculations as given in Fig. 7b variation of the heat flow reaches up to 10 mW/m^2. In the final model given in Fig. 7c, heat production of sedimentary rocks is added to the first two effects. The heat flow value in the basin is calculated as about 65 mW/m^2 which is in agreement with the calculated mean heat flow (65.8 mW/m^2) calculated in this study. According to the thermal model, heat flow in the Strandja massif is around 80 mW/m^2, which is also in agreement with the contour map of Tezcan and Turgay (1991). The difference of about 15 mW/m^2 between the basin and massif heat flow can be explained by the combined effects of differences in the thickness of basement heat production and radioactivity and the effect of thermal refraction to the basin fill. The latter occurs due to the preferential escape of heat from the periphery of the basin due to relatively lower thermal conductivity of the basin fill compared to the higher thermal conductivity of the surrounding crystalline rocks (see Huvaz et al. 2007 for more detail).

Table 3 Thrace Basin 3D model thermal properties

Geological unit	Thermal Conductivity λ (W/m K)	Heat production A(μW/m^3)
Sediments with low thermal conductivity	1.5[a]	0.8
Basin fill	2.5	0.8
Basement/Upper Crust	3.0[b]	2.0[c,d]
Lower Crust	2.0[e]	0.1[e]

Parameter values are derived from [a]Erkan (2015), [b]Balkan et al. (2017), [c]Aysal et al. (2018), [d]Şahin et al. (2014), [e]Blackwell (1971)

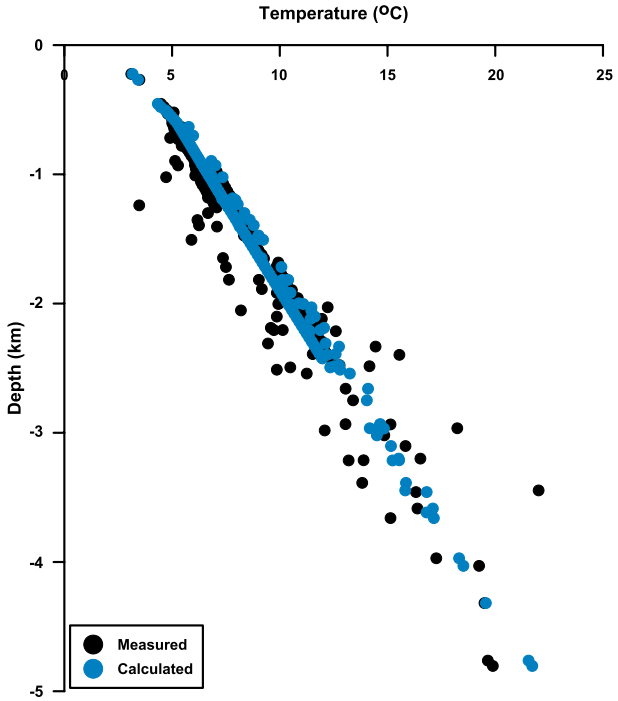

Fig. 6 Comparison between observed and modelled temperatures in Thrace Basin

Conclusions

In this study, we investigated variations of the surface heat flow in the Northern Thrace Basin by combining the available BHT data with the available formation thermal conductivity and thickness information. We calculated the surface heat flow for each BHT point using Bullard's thermal resistance method. The results show an average heat flow of 65.8 ± 11.3 mW/m^2. Our heat flow model emphasizes three regions of high heat flow within the study area that are in the eastern and western sides, and in the central part around Hamitabat. In these areas, heat flow values of 10–20 mW/m^2 higher than the other parts of the basin can have significant effect on the basin temperatures at depth. We calculated formation temperatures in the ranges of 45–64 °C at 1 km depth, 99–136 °C at 3 km depth, and 155–208 °C at 5 km depth for selected hydrocarbon fields in the basin.

Eyerer et al. (2020) calculated the levelized cost of electricity (LCOE) for various geothermal power plants in Germany and showed a dramatic decrease in the LCOE by moderate amounts of increases in reservoir temperatures (30 ct€/kWh at 120 °C, 20 ct€/kWh at 140 °C, 15 ct€/kWh at 160 °C, and below 10 ct€/kWh at 180 °C). The higher subsurface temperatures calculated in this study for some fields can be potential areas for low-cost geothermal energy utilization in the future.

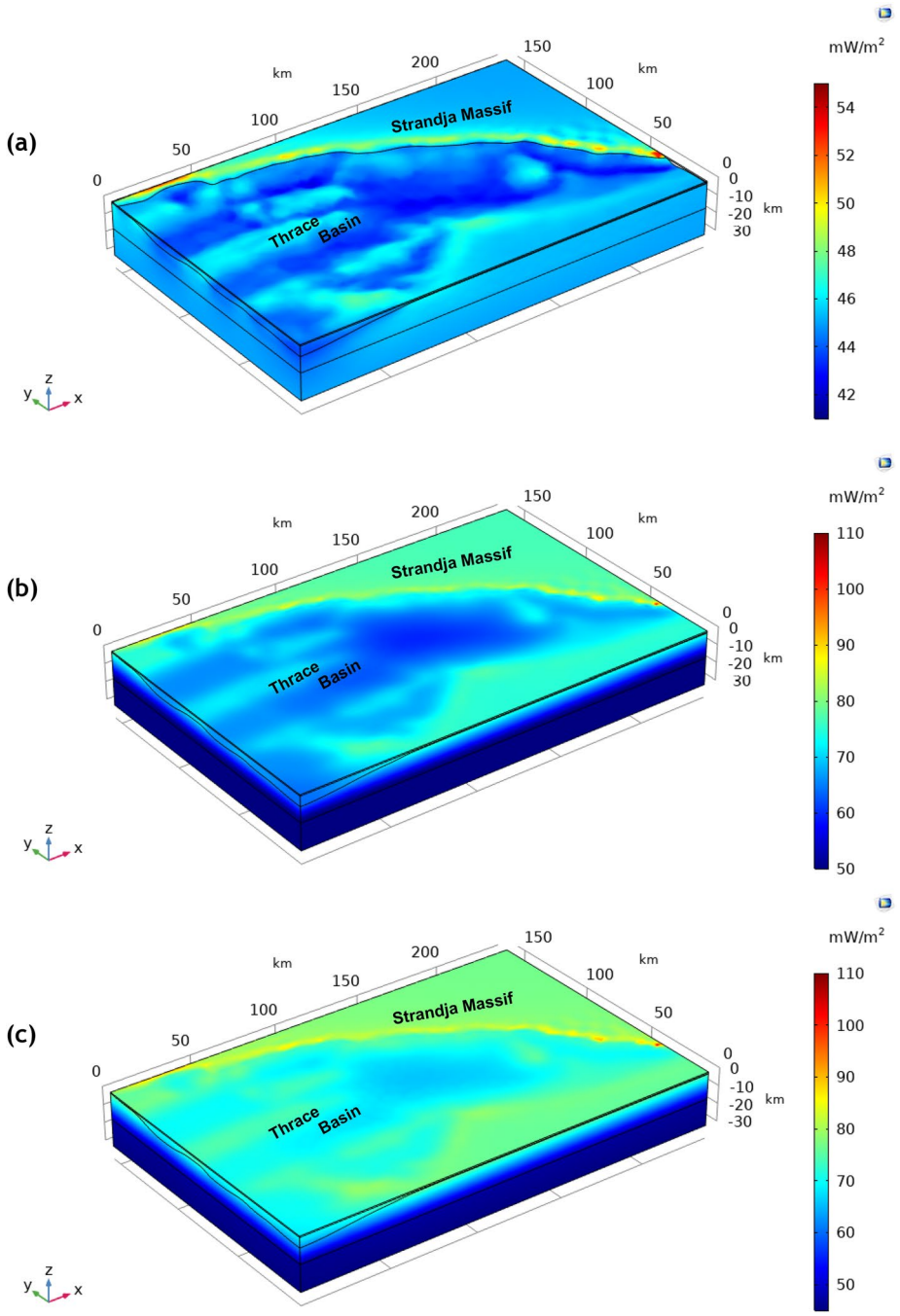

Fig. 7 Conductive thermal modeling of the Thrace basin showing variations of surface heat flow due to the basin structure. Heat flow variations are shown for contributions from **a** mantle heat flow only, **b**) mantle heat flow and basement radioactivity, and **c**) mantle heat flow, basement radioactivity, and basin-fill radioactivity. See the text for details

Appendix

Error propagation method for calculations of subsurface temperatures

Temperature at depth (T) calculations in Table 2 involves surface heat flow Q_s, thermal conductivity of formations (λ), radiogenic heat generation, and they are related with (Jaeger 1965)

$$T(z, Q_s, \lambda, A) = T_s + \frac{Q_s}{\lambda} z - \frac{Az^2}{2\lambda} \tag{4}$$

where T_s is the surface temperature. Assuming no error in depth, error propagation (ΔT) can be calculated as (Chapra and Canale 2010, Page 96)

$$\Delta T = \frac{z}{\lambda}\Delta Q_s + \frac{\left(2Q_s z - Az^2\right)}{2\lambda^2}\Delta\lambda + \frac{z^2}{2\lambda}\Delta A \tag{5}$$

For $\Delta Q_{s,}$ we used the mean of the residual between calculated and measured heat flow from BHT data as 4.7 mW/m^2. For two wells, where equilibrium T–D data are available, we neglected the error in heat flow determination. Since this study uses bulk (A, λ) properties of formations, for ΔT and ΔA, variations in geology is more important than instrumental error; so we assumed variations of 10% for both.

In practice, Eq. (5) can be applied for each layer, where top of the layer is Q_s, and z is the layer thickness. Then, accumulated error in temperature at depth can be integrated from the surface.

Supplementary Information

The online version contains supplementary material available at https://doi.org/10.1186/s40517-023-00253-7.

Additional file 1. Heat flow calculations for each BHT point using Bullard's method.

Acknowledgements
Authors would like to thank to Yağmur Polat and Ilayda Çetinkaya for their help in digitization of the some of the previously published data.

Author contributions
KE analyzed the temperature data from drill holes and calculated heat flow using Bullard s method, also wrote most part of the manuscript. EBP performed the 3D thermal model of the basin. Both authors studied on the interpretation of the equilibrium temperature–depth data and calculated heat flow values. Both authors read and approved the final manuscript.

Funding
Not applicable.

Availability of data and materials
The calculated heat flow data related to this article can be found in the supplementary file.

Declarations

Competing interests
The authors declare that they have no competing interests.

Received: 22 July 2022 Accepted: 10 April 2023
Published online: 19 May 2023

References

Allis R, Gwynn M, Hardwick C, Mines G, Moore J. Will stratigraphic reservoirs provide the next big increase in US geothermal power generation? Geothermal Resources Council Trans. 2015;39:389–98. https://doi.org/10.1016/b978-0-08-100337-4.00013-9.

Ates A, Bilim F, Buyuksarac A, Aydemir A, Bektas O, Aslan Y. Crustal structure of Turkey from aeromagnetic, gravity and deep seismic reflection data. Surv Geophys. 2012;33:869–85. https://doi.org/10.1007/s10712-012-9195-x.

Aysal N, Şahin SY, Güngör Y, Peytcheva I, Öngen S. Middle Permian-Early Triassic magmatism in the Western Pontides, NW Turkey: geodynamic significance for the evolution of the Paleo-Tethys. J Asian Earth Sci. 2018;164:83–103. https://doi.org/10.1016/j.jseaes.2018.06.026.

Balkan E, Erkan K, Şalk M. Thermal conductivity of major rock types in western and central Anatolia regions, Turkey. J Geophys Eng. 2017;14:909–19. https://doi.org/10.1088/1742-2140/aa5831.

Başel EDK, Satman A, Serpen U. Predicted subsurface temperature distribution maps for Turkey. Proceedings World Geothermal Congress, Bali, Indonesia. 2010;pp:25–29.

Beardsmore GR, Cull JP. Crustal heat flow: a guide to measurement and modelling. Cambridge: Cambridge University Press; 2001.

Blackwell DD. The thermal structure of the continental crust. In: The structure and physical properties of the earth's crust, vol. 14. Washington, DC: American Geophysical Union; 1971. p. 169–84. https://doi.org/10.1029/gm014p0169.

Blackwell DD, Steele JL. Thermal conductivity of sedimentary rocks: measurement and significance. In: Naeser ND, McCulloh TH, editors. Thermal history of sedimentary basins. New York: Springer; 1989. p. 13–36. https://doi.org/10.1007/978-1-4612-3492-0_2.

Bullard EC. Heat flow in south Africa. Proc Royal Soc Lond Series A Math Phys Sci. 1939;173(955):474–502. https://doi.org/10.1098/rspa.1939.0159.

Chapman DS. Thermal gradients in the continental crust. Geol Soc Lond Special Publ. 1986;24(1):63–70. https://doi.org/10.1144/GSL.SP.1986.024.01.07.

Chapra SC, Canale RP. Numerical methods for engineers. 6th ed. New York: McGraw-Hill; 2010.

Clark SP, editor. Handbook of physical constants. vol. 97. Geological society of America; 1966.

Coşkun B. Oil and gas fields—transfer zone relationships, Thrace basin, NW Turkey. Marine Petrol Geol. 1997;14:401–16. https://doi.org/10.1016/S0264-8172(96)00062-1.

Coşkun B. Influence of the Istranca-Rhodope Massifs and strands of the North Anatolian Fault on oil potential of Thrace Basin, NW Turkey. J Petrol Sci Eng. 2000;27:1–25. https://doi.org/10.1016/S0920-4105(00)00013-9.

Doust H, Arıkan Y. The geology of the Thrace Basin. Proc. 2nd Petrol Congr. of Turkey, 1974;pp 227–248.

Eppelbaum L, Kutasov I, Pilchin A. Applied geothermics. Heidelberg: Springer; 2014.

Erkan K. Geothermal investigations in western Anatolia using equilibrium temperatures from shallow boreholes. Solid Earth. 2015;6:103–13. https://doi.org/10.5194/se-6-103-2015.

Eyerer S, Schifflechner C, Hofbauer S, Bauer W, Wieland C, Spliethoff H. Combined heat and power from hydrothermal geothermal resources in Germany: an assessment of the potential. Renew Sustain Energy Rev. 2020;120:109661. https://doi.org/10.1016/j.rser.2019.109661.

Förster A, Fuchs S, Förster HJ, Norden B. Ambiguity of crustal geotherms: a thermal-conductivity perspective. Geothermics. 2021;89:101937. https://doi.org/10.1016/j.geothermics.2020.101937.

Görür N, Okay AI. A fore-arc origin for the Thrace Basin, NW Turkey. Geol Rundsch. 1996;85:662–8. https://doi.org/10.1007/BF02440103.

Gürgey K. Geochemical overview and undiscovered gas resources generated from Hamitabat petroleum system in the Thrace Basin, Turkey. Marine Petrol Geology. 2009;26:1240–54. https://doi.org/10.1016/j.marpetgeo.2008.08.007.

Huvaz O. Investigation of the thermal gradient history of the Thrace Basin, NW Turkey, by using a modified easy %Ro maturity model (PhD Dissert.). Middle East Technical University. http://etd.lib.metu.edu.tr/upload/12606250/index.pdf.

Huvaz O, Sarikaya H, Nohut OM. Nature of a regional dogleg pattern in maturity profiles from Thrace basin, northwestern Turkey: A newly discovered unconformity or a thermal anomaly? AAPG Bull. 2005;89:1373–96. https://doi.org/10.1306/06090505021.

Huvaz O, Karahanoglu N, Ediger V. The thermal gradient history of the Thrace Basin, NW Turkey: correlation with basin evolution processes. J Petrol Geology. 2007;30:3–24. https://doi.org/10.1111/j.1747-5457.2007.00003.x.

Jaeger JC. Application of the theory of heat conduction to geothermal measurements. *Terrestrial Heat Flow* (Ed: H.K. Lee), Geophysical Monograph Series Number 8, American Geophysical Union, 1965;7–23.

Jessop AM. Thermal Geophysics, vol. 306. Amsterdam: Elsevier; 1990.

Karabulut H, Paul A, Ergün TA, Hatzfeld D, Childs DM, Aktar M. Long-wavelength undulations of the seismic Moho beneath the strongly stretched Western Anatolia. Geophys J Int. 2013;194:450–64. https://doi.org/10.1093/gji/ggt100.

Kukkonen IT, Jokinen J, Seipold U. Temperature and pressure dependencies of thermal transport properties of rocks: implications for uncertainties in thermal lithosphere models and new laboratory measurements of high-grade rocks in the central Fennoscandian shield. Surv Geophys. 1999;20:33–59. https://doi.org/10.1023/A:1006655023894.

Limberger J, Boxem T, Pluymaekers M, Bruhn D, Manzella A, Calcagno P, Beekman F, Cloetingh S, van Wees JD. Geothermal energy in deep aquifers: a global assessment of the resource base for direct heat utilization. Renew Sustain Energy Rev. 2018;82:961–75. https://doi.org/10.1016/j.rser.2017.09.084.

Lopez S, Hamm V, Le Brun M, Schaper L, Boissier F, Cotiche C, Giuglaris E. 40 years of Dogger aquifer management in Ile-de-France, Paris Basin, France. Geothermics. 2010;39:339–56. https://doi.org/10.1016/j.geothermics.2010.09.005.

Mıhçakan IM, Onur M, Erçelebi SG, Okay A, Yılmazer M. Türkiye yeraltı sıcaklık gradyan dağılımının derin kuyu sıcaklıkları ve variogram analizi kullanılarak haritalanması, TUBİTAK Project No: YDABÇAG-100Y040. 92 pp. 2006. (in Turkish).
Okay A, Satır M, Tüysüz O, Akyüz S, Chen F. The tectonics of the Strandja Massif: late-Variscan and mid-Mesozoic deformation and metamorphism in the northern Aegean. Int J Earth Sci. 2001;90:217–33. https://doi.org/10.1007/s005310000104.
Okay AI, Özcan E, Cavazza W, Okay N, Less G. Basement types, Lower Eocene series, Upper Eocene olistostromes and the initiation of the southern Thrace Basin, NW Turkey. Turk J Earth Sci. 2010;19:1–25. https://doi.org/10.3906/yer-0902-10.
Ökten Ş, Yazıcıgil H. Investigation of safe and sustainable yields for the sandy complex aquifer system in the Ergene River Basin, Thrace Region, Turkey. Turkish J Earth Sci. 2005;14:209–26.
Perinçek D. Possible strand of the North Anatolian Fault in the Thrace Basin, Turkey—an interpretation. AAPG Bull. 1991;75:241–57. https://doi.org/10.1306/0C9B2795-1710-11D7-8645000102C1865D.
Perinçek D, Ataş N, Karatut Ş, Erensoy E. Geological factors controlling potential of lignite beds within the Danişmen Formation in the Thrace Basin. Bull Min Res Exp. 2015;150:77–108. https://doi.org/10.19111/bmre.65462.
Pfister M, Rybach L, Şimşek S. Geothermal reconnaissance of the Marmara Sea region (NW Turkey): surface heat flow density in an area of active continental extension. Tectonophysics. 1998;291:77–89. https://doi.org/10.1016/S0040-1951(98)00032-8.
Şahin SY, Aysal N, Güngör Y, Peytheva I, Neubauer F. Geochemistry and U-Pb zircon geochronology of metagranites in Istranca (Strandja) Zone, NW Pontides, Turkey: implications for the geodynamic evolution of Cadomian orogeny. Gondwana Res. 2014;26(2):755–71. https://doi.org/10.1016/j.gr.2013.07.011.
Şensoy S, Demircan M, Ulupınar U, Balta İ. (Türkiye iklim atlası. Turkish State Meteorological Service (DMİ), Ankara. 2008. (in Turkish).
Siyako M, Huvaz O. Eocene stratigraphic evolution of the Thrace Basin, Turkey. Sed Geol. 2007;198:75–91. https://doi.org/10.1016/j.sedgeo.2006.11.008.
Tester JW, Anderson BJ, Batchelor AS, et al. The future of geothermal energy. Massachusetts Institute of Technology Report No 358. 2006.
Tezcan AK, Turgay MI. Heat flow and temperature distribution in Turkey. In: Cermak V, Haenal R, Zui V, editors. Geothermal Atlas of Europe. Germany: Herman Haack Verlag, Gotha; 1991. p. 84–5.
Turgut S, Eseller G. Sequence stratigraphy, tectonics and depositional history in eastern Thrace Basin, NW Turkey. Mar Pet Geol. 2000;17:61–100. https://doi.org/10.1016/S0264-8172(99)00015-X.
Uzunlar Z. Türkiye yeralti sıcaklık gradyanı dağılımının derin kuyu sıcaklık verileri ve variogram analizi ile belirlenmesi (MS Thesis). Istanbul Technical University (in Turkish). https://polen.itu.edu.tr:8443/server/api/core/bitstreams/90db09c2-557d-485a-b407-514808048326/content.
Yalçın MN. Basin modeling and hydrocarbon exploration. J Petrol Sci Eng. 1991;5:379–98. https://doi.org/10.1016/0920-4105(91)90055-R.
Yılmaz Y, Polat A. Geology and evolution of the Thrace volcanism, Turkey. Acta Vulcanol. 1998;10:293–303.

Publisher's Note